NANO LETTERS

pubs.acs.org/NanoLett Letter

Power Management and Reaction Optimization for a Self-Powered Electrochemical System Driven by a Triboelectric Nanogenerator

Yawei Feng, Xi Liang, Jiajia Han, Kai Han, Tao Jiang,* Hexing Li,* and Zhong Lin Wang*

Cite This: https://doi.org/10.1021/acs.nanolett.1c01152 Read Online

ACCESS | Metrics & More | Article Recommendations | Supporting Information

ABSTRACT: Harvesting distributed and low-quality mechanical energies by triboelectric nanogenerators to power electrochemical reactions is beneficial to electric energy saving and certain applications. However, the conventional self-powered electrochemical process is awkward about the reaction rate, energy conversion efficiency, high-operation frequency, and mismatched impedance. Here we demonstrate an advanced self-powered electrochemical system. In comparison with the conventional system that is inert in activity, the superior power management and electrochemical reaction regulation in tandem make the novel system outstanding for hydrogen peroxide production. In addition to the visible product, an internal current efficiency of 24.6% in the system was achieved. The developed system provides an optimization strategy toward electric energy saving for electrochemical reactions as well as enabling their applications in remote areas by converting environmental mechanical vibrational energy for ecological improvement or recyclable chemical fuel generation.

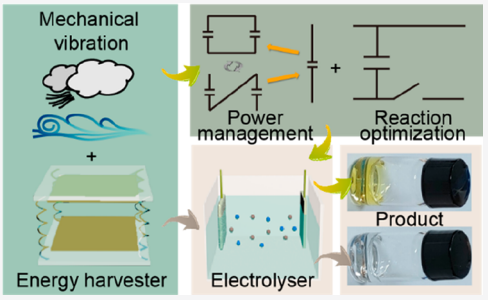

KEYWORDS: *triboelectric nanogenerators, electrochemistry, power management, reaction optimization, self-powered electrochemical system*

An electrochemical route can activate substances in a mild environment to obtain the target products.[1−3] It is an alternative strategy for typical chemical production; however, excessive electric energy is needed to initial the reactions. Converting discrete energies to power specific electrochemical reactions is beneficial to electric energy saving and possesses certain application values.[4−8] Triboelectric nanogenerators (TENGs) have been applied to extract the discrete mechanical energies for the regular operation of micro- or nanosystems by the coupling effect of triboelectrification and electrostatic induction.[9−13] Though they are not invented for electrochemical reactions, there is the possibility of reactions when TENGs are connected with electrochemical cells.

Within a few years after the invention, the TENGs have rapidly developed into a field of self-powered electrochemistry.[14−17] Emerging processes have been reported, such as self-powered water splitting,[18] brine desalination,[19] sterilization,[20] organic component degradation,[21] heavy ion reduction,[22] liquid fuel generation,[23] and nitrogen fixation.[24,25] However, in these works, rotating TENGs with a large number of grid electrodes or contact-separation TENGs (CS-TENGs) with high operation frequency were employed as the direct power sources, which discards the inherent advantages of TENGs for low-frequency vibrational energy harvesting.[26,27] More importantly, there is an impedance contradiction between the harvester and the electrolyzer. As a consequence, negligible or very limited voltage can be applied to the electrolyzer. Although a transformer can enhance the input density to the electrolyzer, this approach is applicable only to the high-frequency operating TENG.[7,21,28] Another feasible strategy is to directly introduce an energy storage unit to intermittently improve the supplied power to the electrolyzer.[29,30] Nevertheless, it is not an efficient method for intensive chemical reactions.

Here, an advanced self-powered electrochemical system (SPECS), consisting of an energy harvester, a power management module, an energy storage module, and an electrolyzer unit, was proposed. Taking the hydrogen peroxide (H_2O_2) production via electrocatalytic oxygen (O_2) reduction as an example, the performance of the SPECS was optimized and demonstrated. The power management in the SPECS does not depend on the input frequency, thus it is universal for all kinds of TENGs. In cooperation with the reaction optimization, H_2O_2 generation was realized by harvesting vibrational energy of 1 Hz. Compared with the conventional self-powered electrochemical (C-SPEC) process with inert activity, the current efficiency reaches about 24.6%, demonstrating the superiority of the constructed SPECS.

To discuss the detailed TENG-powered electrochemical process, a C-SPEC process by combining a rectified CS-TENG

Received: March 24, 2021
Revised: June 12, 2021

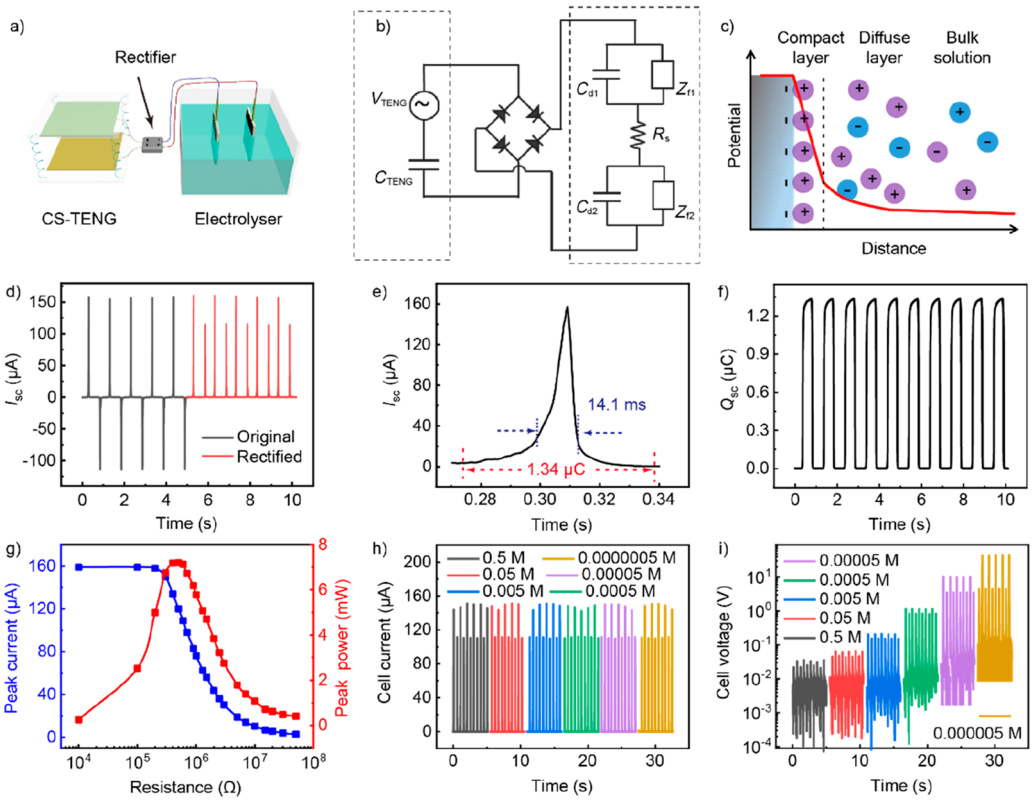

Figure 1. Characterization of the C-SPEC process. Schematic diagram of (a) the C-SPEC system and (b) its equivalent circuit. (c) Diagram showing the EDL at the electrode−solution interface and the potential change along the distance at steady state. (d) I_{SC}, (e) an extracted I_{SC} peak, and (f) Q_{SC} waveform generated by the CS-TENG. (g) Instantaneous peak current and power-resistance relationships of the CS-TENG. (h) Current and (i) voltage supplied to the electrolyzer by the rectified CS-TENG at an operation frequency of 1 Hz.

device and H_2O_2 electrocatalytic generation was constructed, which is schematically shown in Figure 1a. The CS-TENG can be simplified into a hybrid of voltage source and capacitor, while the equivalent circuit of the electrolyzer is more complicated (Figure 1b). The bulk solution is treated as a resistor (R_s) for its function of ionic conductivity. An electric double layer (EDL) capacitor (C_d) exists for the electrode−solution interface, which is contributed from the compact (Helmholtz) and diffuse layers in series (Figure 1c).[31] Although EDL has been known for decades, recently studies found that electron transfer is an initial contributor to its formation.[11,32,33] Due to the intermittent input of the CS-TENG and the frequency dependence of the simulated equivalent circuit, the chemical reaction at the electrode surface is equivalent to a nonlinear Faraday element (Z_f).[34] Figure 1c shows the remarkable potential change along the distance distribution in the stable state. Different from the direct-current (DC)-powered condition, the current waveform in the C-SPEC process is pulsed with an extraordinarily narrow bandwidth. Thus, the potential distribution varies with respect to time and operation frequency.

A CS-TENG with an effective contact area of 100 cm^2 was fabricated as the power source, whose energy conversion mechanism is illustrated in Figure S1. Since CS-TENG exhibits a dominant advantage at low-frequency operation (lower than several Hz), the fabricated device was externally triggered at a fixed frequency of 1 Hz. The peak short-circuit current (I_{SC}, Figure 1d) before or after rectification was recorded to be 158 μA, and the open-circuit voltage (V_{OC}, Figure S2) was estimated to be >1770 V. On the basis of the time (t) integration of the measured current (I_t) (eq 1, Figure 1e) or the direct measured result (Figure 1f), about 1.34 μC of charge (Q_{SC}) was transferred to the separating−contacting process under the short-circuit condition.

$$Q = \int_0^{T/2} I_t \, dt \tag{1}$$

However, the flow of these electrons takes place within only tens of milliseconds, resulting in a noticeable peak with a time span of 14.1 ms (Figure 1e). When loading a resistance of lower than 0.3 MΩ (Figure 1g), the output current exhibits negligible attenuation in intensity relative to I_{SC}, which suggests that CS-TENG is a stable current source under this condition. An instantaneous peak power of 7.2 mW is achieved at the matched resistance of 0.5 MΩ, indicating the giant internal impedance of the CS-TENG.

Modified graphite felt (Figure S3) with qualities of making full use of the dissolved O_2 and high stability and activity was applied as the cathode for H_2O_2 generation. The electrochemical reaction for H_2O_2 generation can be described as a mixed route of a two-electron reduction of O_2 (eq 2) and a subsequent protonation process (eq 3).[7,35]

$$O_2 + 2e^- + H_2O \rightarrow HO_2^- + OH^- \tag{2}$$

$$HO_2^- + H^+ \rightarrow H_2O_2 \tag{3}$$

A series of Na_2SO_4 aqueous solutions with 5 orders of magnitude of molar concentration were prepared for the C-SPEC performance evaluation. The apparent resistances of the above solutions with the sequence from high to low

https://doi.org/10.1021/acs.nanolett.1c01152
Nano Lett. XXXX, XXX, XXX−XXX

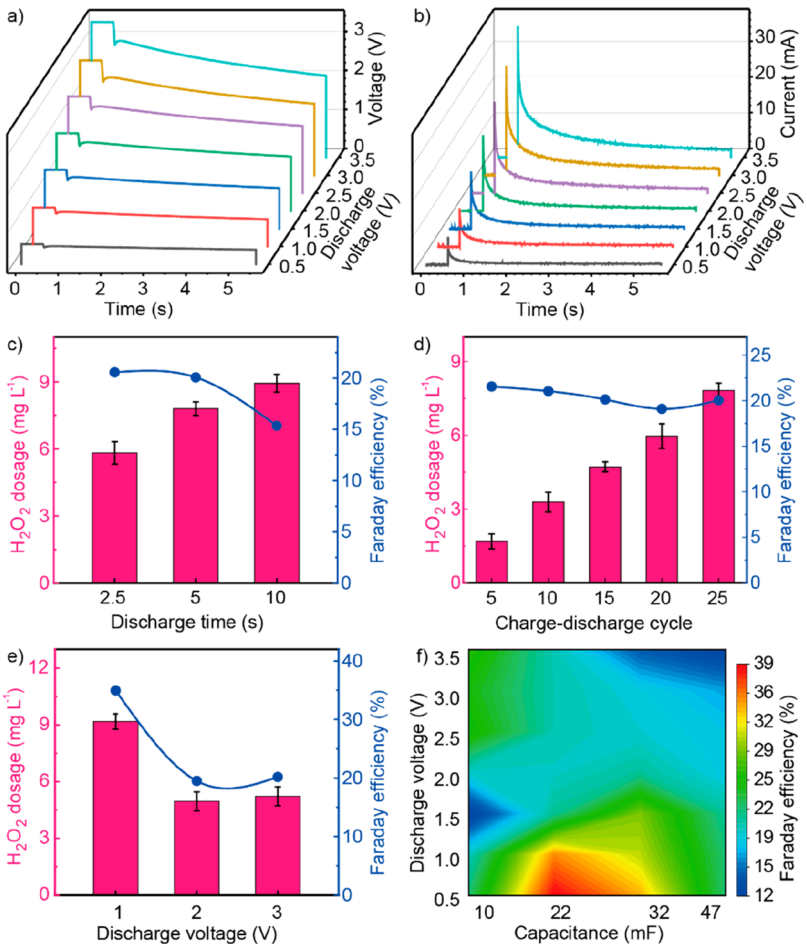

Figure 2. H_2O_2 generation simulation in an electrolyzer with a 0.5 M Na_2SO_4 electrolyte solution by charging−discharging a supercapacitor. (a) Voltage on the electrolyzer and (b) current flowing through the electrolyzer by discharging a 22 mF supercapacitor from different initial voltages. (c) H_2O_2 generation and corresponding Faraday efficiency for different discharge times. All processes were conducted for 25 charge−discharge cycles from 2.0 V. (d) H_2O_2 accumulation and Faraday efficiency over different charge−discharge cycles. (e) The effect of initial voltage on the electrochemical product. A discharge time of 5 s was conducted for each cycle. For the cases of discharging from 1, 2, and 3 V, 50, 25, and 14 charge−discharge cycles were performed, respectively. (f) A Faraday efficiency distribution mapping the experimental results in space of the discharge voltage and supercapacitor capacitance.

concentration are 0.9, 1.7, 3.1, 7.9, and 39 kΩ, respectively, according to the measured results using a Keithley 6514 system electrometer. Evidently, the impedances of the solutions are much lower than the internal impedance of the CS-TENG. When the rectified CS-TENG is connected with an electrolyzer (Figure 1a,h,i), the input current is equivalent to the I_{SC} from the CS-TENG, which has a weak relationship with the Na_2SO_4 concentration. However, the voltage supplied to the electrolyzer exhibits a significant difference. The voltage amplitude varies from tens of millivolts to tens of volts according to the electrolyte concentration. Note that the supplied voltages are insufficient to initiate the reaction (Figure S3f) in the case of high electrolyte concentration, while the potential drop (Figure 1c) would gradually concentrate on the bulk electrolyte with decreasing electrolyte concentration, which provides a small benefit to the interfacial electrochemical reaction. Besides, the charges from the CS-TENG are quite limited. Only 115.8 mC of electrons was transferred by operating the harvester over 12 h. For the comprehensive factors, no target product was obtained after the mentioned operation time.

The above discussions indicate the infeasibility of the C-SPEC scheme by a low-frequency-operating CS-TENG. It is out of balance in the intermittent supplied intensity at hundreds of microamperes and a reaction requirement beyond milliamperes. Thus, power management of the CS-TENG outputs and process optimization for chemical reactions are required. A supercapacitor (22 mF) with no obvious self-discharging phenomenon (Figure S4) was employed as the energy storage unit to intermittently improve the input power to the electrolyzer (0.5 M Na_2SO_4 was used as the electrolyte). As shown in Figures 2a,b and S5, the voltage on the supercapacitor dropped dramatically within 40 ms after conducting the mechanical switch. Unlike the constant current supplied by a DC power source, the supercapacitor voltage change generates a strong current within this period. Taking the case of discharging from 0.5 V as an example, a peak current of 7.8 mA was induced, far exceeding the value (0.13 mA) for the case of being powered by a 0.5 V DC power source. Note that the electrons flowing by the integration of current (Figure 2b, eq 1) are 5−8% smaller than the results calculated with

$$Q = C(V_2 - V_1) \tag{4}$$

where C is the capacitance of the supercapacitor, V_2 is the capacitor voltage after 5 s of discharging, and V_1 is the initial capacitor voltage. This difference may result from the different

https://doi.org/10.1021/acs.nanolett.1c01152
Nano Lett. XXXX, XXX, XXX−XXX

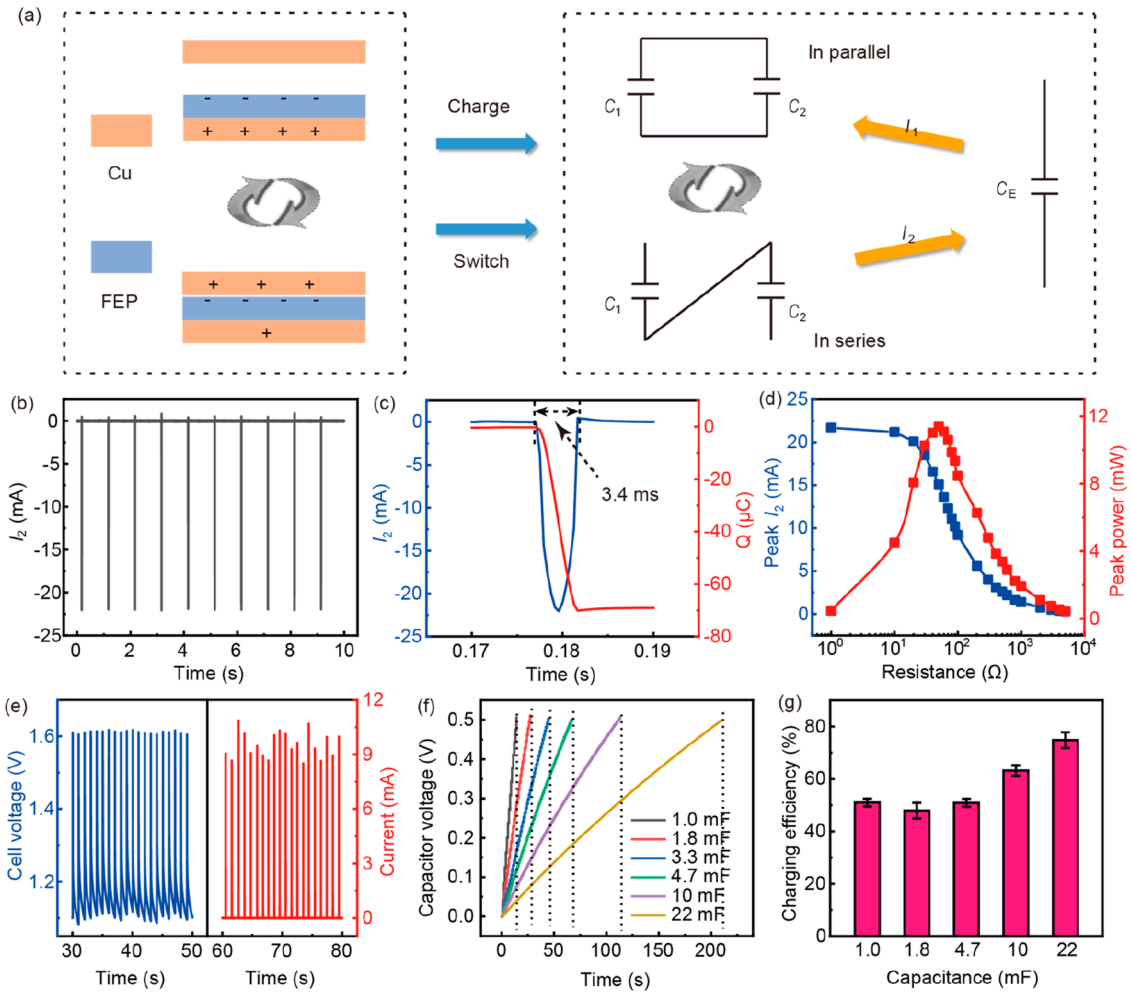

Figure 3. Performance of the power-managed TENG array. (a) Schematic diagram showing the power management principle for the CS-TENG array. (b) Current waveform from channel 2 of the CEC without loaded resistance. (c) Enlarged view of an individual I_2 peak and the corresponding transferred charges for this period. (d) Instantaneous peak current and power-resistance relationships of the managed CS-TENG array. (e) Voltage and current supplied to the electrolyzer, (f) charging performance, and (g) charging efficiency for different capacitances by the CS-TENG array integrated with the CEC.

measurement principles of the electrometer (for voltage profile) and electrochemical workstation (for the current profile).

The intensive discharge mainly occurs in the initial stage, followed by a slow-release process. Meanwhile, it takes some time for H_2O_2 generation (eqs 2 and 3) and diffusion from the electrode−solution interface to the bulk solution. Hence, the discharging time was first optimized (Figure 2c). At 2 V of initial discharge voltage, the yield increases with the increasing discharge time, which means that more electrons are involved in the reaction. The Faraday efficiency (FE) of H_2O_2 evolution was calculated by

$$\mathrm{FE} = \frac{nFCV}{MQ} \tag{5}$$

where n is the transferred electron number for O_2 reduction to H_2O_2 ($n = 2$), F is the Faraday constant (96 486 C/mol), C is the H_2O_2 concentration (only in eq 5, g L^{-1}), V is the solution volume (L), M is the molar mass of H_2O_2 (34.01 g mol^{-1}), and Q is the input electron amount calculated by eq 4. Excessive discharge leads to electron waste and a lower FE. Thus, an appropriate discharge span (5 s) was selected for the subsequent experiments. The H_2O_2 molecules are accumulated almost linearly as the function of charge−discharge cycles (0.31 mg (L cycle)$^{-1}$) with the Faraday efficiency of 20.1% (Figure 2d). This efficiency is much smaller than for the DC-powered case (65% FE) under the same reaction conditions,[9] which may result from the faster voltage decrease and electron loss at the lower voltage.

The results in Figure 2e,f and Table S1 indicate that the optimization condition under the neutral condition is to discharge a 22 mF supercapacitor over 5 s at the initial voltage of 0.5 V. As for the traditional electrochemistry, −0.5 V of constant potential vs the Pt electrode is impossible to drive the O_2 reduction reaction. However, when powered by a discharging supercapacitor, the flowing current can reach 7.8 mA, far exceeding the steady-state intensity of 0.13 mA, which should be responsible for the reaction possibility. Under the optimized discharge conditions, about 0.142 mg L^{-1} of H_2O_2 was generated per cycle, and the highest FE of 38.7% was achieved.

The power management of CS-TENG was referenced to our previous work,[36] and its working principle is demonstrated in Figure 3a. This power management module is a voltage-multiplying-based charge excitation circuit (CEC, Figure S6a,b). The main part of the CEC is a capacitor set composed

https://doi.org/10.1021/acs.nanolett.1c01152
Nano Lett. XXXX, XXX, XXX−XXX

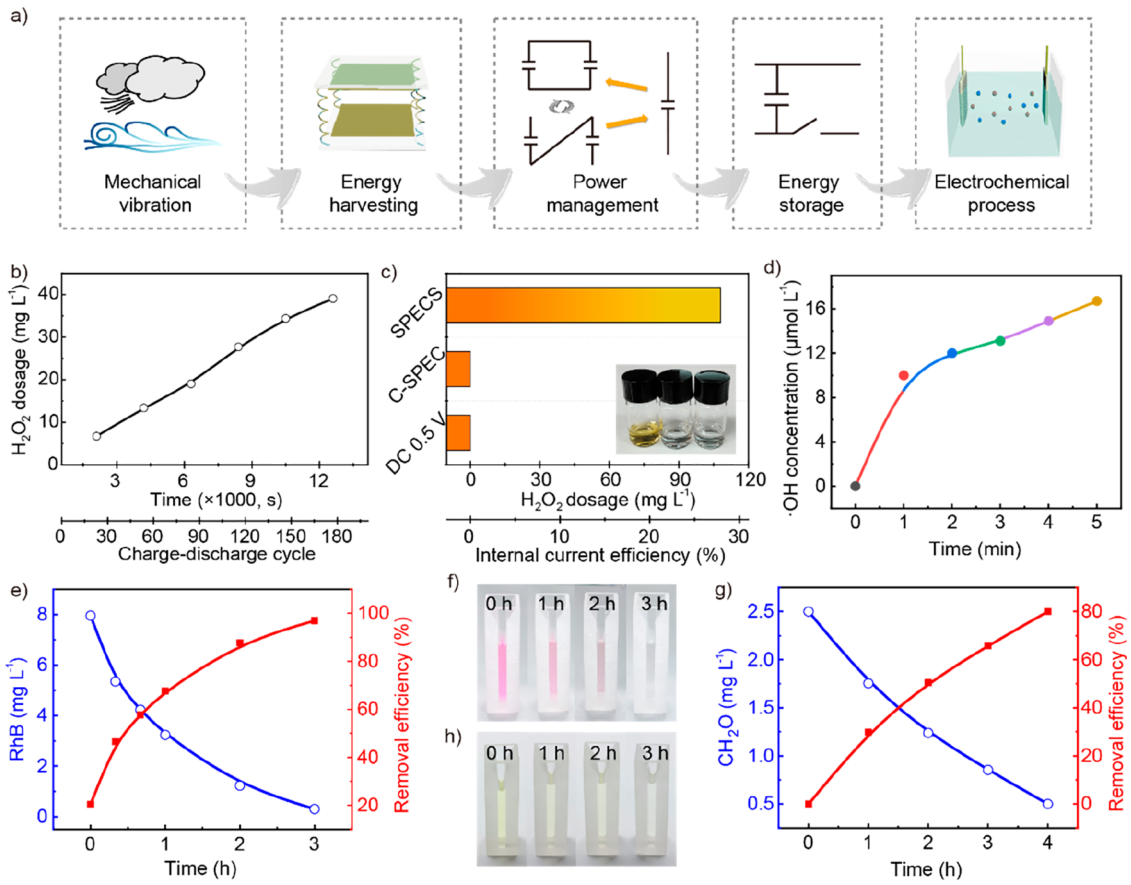

Figure 4. Performance and application of the SPECS. (a) Framework of the SPECS. (b) H_2O_2 accumulation process over time and the charge−discharge cycle by the SPECS. (c) Comparison of the product generation and internal current efficiency among the SPECS, C-SPEC process, and DC-source-powering process. The inset picture shows the developed solution with a chromogenic reagent, indicating the obtained H_2O_2 dosages by different methods. (d) ·OH generation over time by catalytic H_2O_2 decomposition. (e, f) RhB and (g, h) CH_2O concentration variations and removal efficiency as functions of time. The red color in (f) is the RhB color, and the yellow color in (h) denotes that the CH_2O solution reacted with acetylacetone.

of two identical capacitors C_1 and C_2 (both 10 μF). Two N-type metal oxide−semiconductor field-effect transistors (MOSFETs, M_1 and M_3 in Figure S6b) and one P-type MOSFET (M_2 in Figure S6b) were applied to realize the automatic switch function of the two capacitors from parallel to series connection. The normal work of the CEC is not dependent on the TENG mode and its operation frequency, thus it is a universal management strategy. The CS-TENG discussed in Figure 1 easily breaks down the MOSFETs, thus an array composed of nine smaller CS-TENG units (3 cm × 3 cm, Figure S7) was fabricated to reduce the overall input voltage. In order to realize a complete loop, an external capacitor C_E of 1 mF was introduced. When the CEC is connected, the alternating current output from the TENG array can not only be directly converted to the DC without a rectifier bridge but also can be increased by several times (Figure S6c). The measured peak value of I_2 (Figure 3b) is significantly enhanced over the original output from the CS-TENG array (Figure S7c), which is as high as 21.9 mA. On the basis of the integral calculation (Figure 3c), 69.1 μC of charge is transferred per operation cycle, which is 24.7 times the Q_{SC} from the rectified array. The peak power-resistance profile in Figure 3d indicates the optimal matched resistance of 50 Ω, which is significantly shrunken compared to the 0.5 MΩ unmanaged CE-TENG, accompanied by 1.6 times (11.4 mW) the instantaneous peak power output in Figure 1g.

Managed by this CEC, the voltage and current supplied to the electrolyzer are greatly improved. As depicted in Figure 3e, the voltage and current input into the electrolyzer are both pulsed waveforms. The pulsed voltage has a baseline of 1.1 V with a peak value of 1.6 V, and the peak current changes range from 8.8 to 10.6 mA. Note that it needs about 20 s to form the stable voltage waveform (Figure S9) when powered by the managed CS-TENG array, which may be associated with the EDL formation on the electrode−solution interface (Figure 1c). However, due to the fast switching of the capacitor set, the apparent time input into the electrolyzer is several milliseconds (Figure S10), which is even shorter than the pulse span of I_2 regardless of the square-wave voltage signal U_{out} (Figure S8) on the open-state output channel. According to the previous report, the pulsed current with such a short time in the electrolyzer is not beneficial to the electrocatalytic production of H_2O_2.[37]

Therefore, the strategy for charging and discharging a capacitor is adopted. Since the maximum potential difference on the output channel is no more than 3 V (Figure S8), the charging speed of the 1 mF capacitor decreases rapidly with the increasing capacitor voltage (Figure S11). To charge the capacitors to the optimum value (0.5 V), 14, 27, 45, 66, 113, and 210 s are needed for capacitors of 1.0, 1.8, 3.3, 4.7, 10, and 22 mF, respectively. The charging efficiency (CE) from the CEC to the capacitor is described by

https://doi.org/10.1021/acs.nanolett.1c01152
Nano Lett. XXXX, XXX, XXX−XXX

$$CE = \frac{Q_c}{Q_i} \quad (6)$$

where Q_c is the stored charges at a capacitor voltage of 0.5 V, which can be obtained by eq 4, and Q_i is the total charge transferred from the CEC. Figure 3g shows a constant efficiency of about 50% to charge the electrolytic capacitors (1.0, 1.8, 3.3, and 4.7 mF) and the highest efficiency of about 75% for the 22 mF supercapacitor.

On the basis of the above discussions, a SPECS was constructed as illustrated in Figure 4a and Figure S12 and used as a H_2O_2 generator. In this system, the CS-TENG array (Figure S7) with an operation frequency of 1 Hz is employed as the energy harvester to convert mechanical vibration into electrical energy; the sealed power management module (Figure S6, the black box in Figure S12) is used to amplify the output performance of the TENG array; a supercapacitor (22 mF) is utilized to store the output energy from the CEC with the function to improve the input density to the electrolyzer under the assistance of a mechanical switch; and the printed container with a cover to hold the electrodes serves as the electrolyzer, with a hole reserved on the cover to facilitate the natural diffusion of air. The electrolyzer including the vessel and cover was treated with a hydrophobic coating to restrain the water loss (Figure S13a).

Electrocatalytic H_2O_2 generation by the SPECS was intermittently performed. Although it takes 210 s for the 22 mF supercapacitor to be charged to 0.5 V from the completely discharged stage (Figure 3f), discharging of 5 s from 0.5 V causes the capacitor voltage to decrease to 0.37 V (Figure 2a). Hence, discharge once releases about 3.0 mC of charge, and it takes less than 70 s to realize a charge−discharge cycle. The accumulated H_2O_2 product dosage increases almost linearly with the charge−discharge cycle number, which is plotted in Figure 4b. Although the H_2O_2 concentration reaches 25.4 mg L^{-1} after the SPECS operates for 180 cycles, it is insufficient to carry out some valuable chemical reactions. Therefore, the operation time was greatly extended, aiming at a dosage. Owing to the excellent cathode stability, the concentration of H_2O_2 product reached 108 mg L^{-1} after 15 h of operation. The overall conversion efficiency of the SPECS should take the harvesting efficiency of the CS-TENG, the management efficiency of the power management module, and the Faraday efficiency of electrochemical reactions into consideration. However, the harvesting efficiency of mechanical energy is difficult to quantify in the given case. Accordingly, the internal current efficiency involving the number of electrons for H_2O_2 production in theory and the charge amount output from the CEC is used to evaluate the merit of the SPECS, which is calculated to be 24.6%. In contrast, 60 h of the C-SPEC process by the CS-TENG array and 0.5 h of the 0.5 V DC-source-powering process showed inert performance for H_2O_2 generation (Figure 4c).

The obtained aqueous product by the SPECS has the same chemical property for reactions as that of the normal reagent. For the well-known reaction of H_2O_2, subsequent application of the Fenton reaction was demonstrated. For the generation of active species ·OH via catalytic H_2O_2 decomposition, Cu-anchored carbon nitride ($Cu-C_3N_4$) was prepared (Figure S14). The generation of active ·OH and the circulation of the $Cu-C_3N_4$ catalyst are presented by

$$Cu^+ + H_2O_2 \rightarrow Cu^{2+} + \cdot OH + OH^- \quad (7)$$

$$Cu^{2+} + H_2O_2 \rightarrow Cu^+ + \cdot HO_2 + H^+ \quad (8)$$

The fluorescence emission spectra (Figure S15) show the rapid production of free radicals (Figure 4d), which can also support the degradation mechanism in subsequent organic removal. The absorption spectra (Figures S16 and S17), substrate removal efficiency (Figure 4e,g), and photographs of the centrifuged solution (Figure 4f,h) exhibit the variations in organic compound concentration with respect to time.

In conclusion, an advanced self-powered electrochemical system, including an energy harvester, a power management module, an energy storage module, and an electrolyzer unit, was designed. By power management and reaction optimization, self-powered H_2O_2 generation by electrocatalytic O_2 reduction was achieved by harvesting low-frequency mechanical vibration at 1 Hz using TENG. Besides the same function of the obtained aqueous product by the SPECS analogy to chemical reactions using normal reagents, an internal current efficiency of 24.6% from the managed TENG to the electrochemical product was attained, indicating the preponderance of the SPECS in comparison with the inert performance of the conventional self-powered process. The management and optimization strategy of the SPECS developed in this work does not depend on the frequency of the input mechanical energy, so it is universal for both low- and high-frequency energy conversion. The superiority of the SPECS makes it easier to extend its application to electrochemistry, especially its potential application in remote areas by converting environmental mechanical vibrational energy.

■ ASSOCIATED CONTENT

Supporting Information

The Supporting Information is available free of charge at https://pubs.acs.org/doi/10.1021/acs.nanolett.1c01152.

Additional methods showing the preparation of CS-TENG and catalysts, the measurement of H_2O_2, the degradation of organic compounds, a table showing the results powered by a different supercapacitor, and figures showing the energy output mechanism, catalyst characterization, discharge characterization, performance of the managed array, and organics degradation performance (PDF)

■ AUTHOR INFORMATION

Corresponding Authors

Tao Jiang − *CAS Center for Excellence in Nanoscience, Beijing Key Laboratory of Micro-Nano Energy and Sensor, Beijing Institute of Nanoenergy and Nanosystems, Chinese Academy of Sciences, Beijing 101400, China; School of Nanoscience and Technology, University of Chinese Academy of Sciences, Beijing 100049, China*; Email: jiangtao@binn.cas.cn

Hexing Li − *School of Environmental and Chemical Engineering, Shanghai University of Electric Power, Shanghai 200090, China*; orcid.org/0000-0002-3558-5227; Email: hexing-li@shnu.edu.cn

Zhong Lin Wang − *CAS Center for Excellence in Nanoscience, Beijing Key Laboratory of Micro-Nano Energy and Sensor, Beijing Institute of Nanoenergy and Nanosystems, Chinese Academy of Sciences, Beijing 101400, China; School of Nanoscience and Technology, University of Chinese Academy of Sciences, Beijing 100049, China; School of Materials Science and Engineering, Georgia Institute of Technology,*

https://doi.org/10.1021/acs.nanolett.1c01152
Nano Lett. XXXX, XXX, XXX−XXX

Atlanta, Georgia 30332-0245, United States; orcid.org/0000-0002-5530-0380; Email: zlwang@gatech.edu

Authors

Yawei Feng − *CAS Center for Excellence in Nanoscience, Beijing Key Laboratory of Micro-Nano Energy and Sensor, Beijing Institute of Nanoenergy and Nanosystems, Chinese Academy of Sciences, Beijing 101400, China; School of Nanoscience and Technology, University of Chinese Academy of Sciences, Beijing 100049, China*

Xi Liang − *CAS Center for Excellence in Nanoscience, Beijing Key Laboratory of Micro-Nano Energy and Sensor, Beijing Institute of Nanoenergy and Nanosystems, Chinese Academy of Sciences, Beijing 101400, China; School of Nanoscience and Technology, University of Chinese Academy of Sciences, Beijing 100049, China*

Jiajia Han − *CAS Center for Excellence in Nanoscience, Beijing Key Laboratory of Micro-Nano Energy and Sensor, Beijing Institute of Nanoenergy and Nanosystems, Chinese Academy of Sciences, Beijing 101400, China; School of Nanoscience and Technology, University of Chinese Academy of Sciences, Beijing 100049, China*

Kai Han − *CAS Center for Excellence in Nanoscience, Beijing Key Laboratory of Micro-Nano Energy and Sensor, Beijing Institute of Nanoenergy and Nanosystems, Chinese Academy of Sciences, Beijing 101400, China*

Complete contact information is available at: https://pubs.acs.org/10.1021/acs.nanolett.1c01152

Notes

The authors declare no competing financial interest.

■ ACKNOWLEDGMENTS

Support from the National Key R&D Project from the Minister of Science and Technology (2016YFA0202704), the National Natural Science Foundation of China (grant nos. 51432005, 51702018, and 51561145021), and the Youth Innovation Promotion Association, CAS, is appreciated.

■ REFERENCES

(1) Stamenkovic, V. R.; Strmcnik, D.; Lopes, P. P.; Markovic, N. M. Energy and fuels from electrochemical interfaces. *Nat. Mater.* **2017**, *16*, 57−69.

(2) Seh, Z. W.; Kibsgaard, J.; Dickens, C. F.; Chorkendorff, I.; Norskov, J. K.; Jaramillo, T. F. Combining theory and experiment in electrocatalysis: Insights into materials design. *Science* **2017**, *355*, No. eaad4998.

(3) Meyer, T. H.; Choi, I.; Tian, C.; Ackermann, L. Powering the Future: How Can Electrochemistry Make a Difference in Organic Synthesis? *Chem.* **2020**, *6*, 2484−2496.

(4) Fu, H. C.; Varadhan, P.; Lin, C. H.; He, J. H. Spontaneous solar water splitting with decoupling of light absorption and electrocatalysis using silicon back-buried junction. *Nat. Commun.* **2020**, *11*, 3930.

(5) Wang, X.; Huang, Y.-T.; Liu, C.; Mu, K.; Li, K. H.; Wang, S.; Yang, Y.; Wang, L.; Su, C.-H.; Feng, S.-P. Direct thermal charging cell for converting low-grade heat to electricity. *Nat. Commun.* **2019**, *10*, 4151.

(6) Wu, H.; Xu, L.; Wang, Y.; Zhang, T.; Zhang, H.; Bowen, C. R.; Wang, Z. L.; Yang, Y. Enhanced Power Generation from the Interaction between Sweat and Electrodes for Human Health Monitoring. *ACS Energy Lett.* **2020**, *5*, 3708−3717.

(7) Feng, Y.; Han, K.; Jiang, T.; Bian, Z.; Liang, X.; Cao, X.; Li, H.; Wang, Z. L. Self-powered electrochemical system by combining Fenton reaction and active chlorine generation for organic contaminant treatment. *Nano Res.* **2019**, *12*, 2729−2735.

(8) Zhai, N.; Wen, Z.; Chen, X.; Wei, A.; Sha, M.; Fu, J.; Liu, Y.; Zhong, J.; Sun, X. Blue Energy Collection toward All-Hours Self-Powered Chemical Energy Conversion. *Adv. Energy Mater.* **2020**, *10*, 2001041.

(9) Fan, F.-R.; Tian, Z.-Q.; Lin Wang, Z. Flexible triboelectric generator. *Nano Energy* **2012**, *1*, 328−334.

(10) Wang, Z. L. On Maxwell's displacement current for energy and sensors: the origin of nanogenerators. *Mater. Today* **2017**, *20*, 74−82.

(11) Wang, Z. L.; Wang, A. C. On the origin of contact-electrification. *Mater. Today* **2019**, *30*, 34−51.

(12) Wang, Z. L. On the first principle theory of nanogenerators from Maxwell's equations. *Nano Energy* **2020**, *68*, 104272.

(13) Shi, Y.; Wang, F.; Tian, J.; Li, S.; Fu, E.; Nie, J.; Lei, R.; Ding, Y.; Chen, X.; Wang, Z. L. Self-powered electro-tactile system for virtual tactile experiences. *Sci. Adv.* **2021**, *7*, No. eabe2943.

(14) Cao, X.; Jie, Y.; Wang, N.; Wang, Z. L. Triboelectric Nanogenerators Driven Self-Powered Electrochemical Processes for Energy and Environmental Science. *Adv. Energy Mater.* **2016**, *6*, 1600665.

(15) Zhu, G.; Pan, C.; Guo, W.; Chen, C.-Y.; Zhou, Y.; Yu, R.; Wang, Z. L. Triboelectric-Generator-Driven Pulse Electrodeposition for Micropatterning. *Nano Lett.* **2012**, *12*, 4960−4965.

(16) Guo, W.; Li, X.; Chen, M.; Xu, L.; Dong, L.; Cao, X.; Tang, W.; Zhu, J.; Lin, C.; Pan, C.; Wang, Z. L. Electrochemical Cathodic Protection Powered by Triboelectric Nanogenerator. *Adv. Funct. Mater.* **2014**, *24*, 6691−6699.

(17) Feng, Y.; Ling, L.; Nie, J.; Han, K.; Chen, X.; Bian, Z.; Li, H.; Wang, Z. L. Self-Powered Electrostatic Filter with Enhanced Photocatalytic Degradation of Formaldehyde Based on Built-in Triboelectric Nanogenerators. *ACS Nano* **2017**, *11*, 12411−12418.

(18) Tang, W.; Han, Y.; Han, C. B.; Gao, C. Z.; Cao, X.; Wang, Z. L. Self-Powered Water Splitting Using Flowing Kinetic Energy. *Adv. Mater.* **2015**, *27*, 272−276.

(19) Jiang, Q.; Han, Y.; Tang, W.; Zhu, H.; Gao, C.; Chen, S.; Willander, M.; Cao, X.; Lin Wang, Z. Self-powered seawater desalination and electrolysis using flowing kinetic energy. *Nano Energy* **2015**, *15*, 266−274.

(20) Jiang, Q.; Jie, Y.; Han, Y.; Gao, C.; Zhu, H.; Willander, M.; Zhang, X.; Cao, X. Self-powered electrochemical water treatment system for sterilization and algae removal using water wave energy. *Nano Energy* **2015**, *18*, 81−88.

(21) Chen, S.; Wang, N.; Ma, L.; Li, T.; Willander, M.; Jie, Y.; Cao, X.; Wang, Z. L. Triboelectric Nanogenerator for Sustainable Wastewater Treatment via a Self-Powered Electrochemical Process. *Adv. Energy Mater.* **2016**, *6*, 1501778.

(22) Zhou, L.; Liu, D.; Li, S.; Yin, X.; Zhang, C.; Li, X.; Zhang, C.; Zhang, W.; Cao, X.; Wang, J.; Wang, Z. L. Effective removing of hexavalent chromium from wasted water by triboelectric nano-generator driven self-powered electrochemical system − Why pulsed DC is better than continuous DC? *Nano Energy* **2019**, *64*, 103915.

(23) Leung, S. F.; Fu, H. C.; Zhang, M. L.; Hassan, A. H.; Jiang, T.; Salama, K. N.; Wang, Z. L.; He, J. H. Blue energy fuels: converting ocean wave energy to carbon-based liquid fuels via CO_2 reduction. *Energy Environ. Sci.* **2020**, *13*, 1300−1308.

(24) Wong, M. C.; Xu, W.; Hao, J. Microplasma-Discharge-Based Nitrogen Fixation Driven by Triboelectric Nanogenerator toward Self-Powered Mechano-Nitrogenous Fertilizer Supplier. *Adv. Funct. Mater.* **2019**, *29*, 1904090.

(25) Han, K.; Luo, J.; Chen, J.; Chen, B.; Xu, L.; Feng, Y.; Tang, W.; Wang, Z. L. Self-powered ammonia synthesis under ambient conditions via N_2 discharge driven by Tesla turbine triboelectric nanogenerators. *Microsyst. Nanoeng.* **2021**, *7*, 7.

(26) Zhao, J.; Zhen, G.; Liu, G.; Bu, T.; Liu, W.; Fu, X.; Zhang, P.; Zhang, C.; Wang, Z. L. Remarkable merits of triboelectric nanogenerator than electromagnetic generator for harvesting small-amplitude mechanical energy. *Nano Energy* **2019**, *61*, 111−118.

(27) Feng, Y.; Liang, X.; An, J.; Jiang, T.; Wang, Z. L. Soft-contact cylindrical triboelectric-electromagnetic hybrid nanogenerator based

on swing structure for ultra-low frequency water wave energy harvesting. *Nano Energy* **2021**, *81*, 105625.
(28) Yeh, M.-H.; Guo, H.; Lin, L.; Wen, Z.; Li, Z.; Hu, C.; Wang, Z. L. Rolling Friction Enhanced Free-Standing Triboelectric Nanogenerators and their Applications in Self-Powered Electrochemical Recovery Systems. *Adv. Funct. Mater.* **2016**, *26*, 1054−1062.
(29) Yang, Y.; Zhang, H.; Lee, S.; Kim, D.; Hwang, W.; Wang, Z. L. Hybrid Energy Cell for Degradation of Methyl Orange by Self-Powered Electrocatalytic Oxidation. *Nano Lett.* **2013**, *13*, 803−808.
(30) Yang, Y.; Zhang, H.; Lin, Z.-H.; Liu, Y.; Chen, J.; Lin, Z.; Zhou, Y. S.; Wong, C. P.; Wang, Z. L. A hybrid energy cell for self-powered water splitting. *Energy Environ. Sci.* **2013**, *6*, 2429−2434.
(31) Le, J. B.; Fan, Q. Y.; Li, J. Q.; Cheng, J. Molecular origin of negative component of Helmholtz capacitance at electrified Pt(111)/water interface. *Sci. Adv.* **2020**, *6*, No. eabb1219.
(32) Lin, S.; Xu, L.; Chi Wang, A.; Wang, Z. L. Quantifying electron-transfer in liquid-solid contact electrification and the formation of electric double-layer. *Nat. Commun.* **2020**, *11*, 399.
(33) Zhan, F.; Wang, A. C.; Xu, L.; Lin, S.; Shao, J.; Chen, X.; Wang, Z. L. Electron Transfer as a Liquid Droplet Contacting a Polymer Surface. *ACS Nano* **2020**, *14*, 17565−17573.
(34) Bard, A. J.; Faulkner, L. R. *Electrochemical Methods: Fundamentals and Applications*, 2nd ed.; Wiley: New York, 2001; p 376.
(35) Agladze, G. R.; Tsurtsumia, G. S.; Jung, B. I.; Kim, J. S.; Gorelishvili, G. Comparative study of hydrogen peroxide electrogeneration on gas-diffusion electrodes in undivided and membrane cells. *J. Appl. Electrochem.* **2007**, *37*, 375−383.
(36) Liang, X.; Jiang, T.; Feng, Y. W.; Lu, P. J.; An, J.; Wang, Z. L. Triboelectric Nanogenerator Network Integrated with Charge Excitation Circuit for Effective Water Wave Energy Harvesting. *Adv. Energy Mater.* **2020**, *10*, 2002123.
(37) Zhou, W.; Gao, J.; Kou, K.; Meng, X.; Wang, Y.; Ding, Y.; Xu, Y.; Zhao, H.; Wu, S.; Qin, Y. Highly efficient H_2O_2 electrogeneration from O_2 reduction by pulsed current: Facilitated release of H_2O_2 from porous cathode to bulk. *J. Taiwan Inst. Chem. Eng.* **2018**, *83*, 59−63.

https://doi.org/10.1021/acs.nanolett.1c01152
Nano Lett. XXXX, XXX, XXX−XXX